

Contract No : 064065

Synthesis of Si nanowires for an anode material of Li batteries

Principal Investigator :

Kun-Hong Lee, Ph.D.

Professor of chemical engineering,
Pohang university of science and technology
San 31, Hyoja-Dong, Nam-Gu, Pohang, Gyeongbuk, South Korea

TEL : 82-54-279-2271

FAX : 82-54-279-8298

e-mail : ce20047@postech.ac.kr

Report Documentation Page

Form Approved
OMB No. 0704-0188

Public reporting burden for the collection of information is estimated to average 1 hour per response, including the time for reviewing instructions, searching existing data sources, gathering and maintaining the data needed, and completing and reviewing the collection of information. Send comments regarding this burden estimate or any other aspect of this collection of information, including suggestions for reducing this burden, to Washington Headquarters Services, Directorate for Information Operations and Reports, 1215 Jefferson Davis Highway, Suite 1204, Arlington VA 22202-4302. Respondents should be aware that notwithstanding any other provision of law, no person shall be subject to a penalty for failing to comply with a collection of information if it does not display a currently valid OMB control number.

1. REPORT DATE 04 DEC 2007			2. REPORT TYPE Final			3. DATES COVERED 28-06-2006 to 01-11-2007		
4. TITLE AND SUBTITLE Synthesis of Si nanowires for anode material of Li batteries					5a. CONTRACT NUMBER FA48690610092			
					5b. GRANT NUMBER			
					5c. PROGRAM ELEMENT NUMBER			
6. AUTHOR(S) Kun-Hong Lee					5d. PROJECT NUMBER			
					5e. TASK NUMBER			
					5f. WORK UNIT NUMBER			
7. PERFORMING ORGANIZATION NAME(S) AND ADDRESS(ES) Pohang University of Science and Technology, San 31, Hyoja-Dong, Nam-Gu, Gyeongbuk 790-784, Korea (South), KS, N/A					8. PERFORMING ORGANIZATION REPORT NUMBER N/A			
9. SPONSORING/MONITORING AGENCY NAME(S) AND ADDRESS(ES) AOARD, UNIT 45002, APO, AP, 96337-5002					10. SPONSOR/MONITOR'S ACRONYM(S) AOARD-064065			
					11. SPONSOR/MONITOR'S REPORT NUMBER(S)			
12. DISTRIBUTION/AVAILABILITY STATEMENT Approved for public release; distribution unlimited								
13. SUPPLEMENTARY NOTES								
14. ABSTRACT The work encompassed the study of new alloy anode material for the next generation of Li ion battery. The alloy includes Li alloy with Sn, Al and Si. It has been reported that the Li_{4.4}Si alloy can have the theoretical capacity of 4200 mAh/g, which is much higher than the capacity of the graphite. However, in spite of the theoretical prediction, the immense volume increase, thus capacitance decrease occurred during charging and discharging. Therefore, the work focused on the study of morphological and volume change of the Li Si alloy electrodes. The result of the study is expected to contribute to the future work of the Li alloy anode development for the improved capacitance.								
15. SUBJECT TERMS								
16. SECURITY CLASSIFICATION OF:				17. LIMITATION OF ABSTRACT		18. NUMBER OF PAGES	19a. NAME OF RESPONSIBLE PERSON	
a. REPORT unclassified	b. ABSTRACT unclassified	c. THIS PAGE unclassified		Same as Report (SAR)		30		

Contents

Chapter 1. INTRODUCTION	-----	1
Chapter 2. SILICON THIN FILM ANODES	-----	2
Chapter 3. SILICON NANOWIRES AS AN ANODE MATERIAL OF LITHIUM BATTERIES		
3.1. Introduction	-----	13
3.2. Synthesis of Si nanowires from Si wafers	-----	13
3.3. Synthesis of Si nanowires from Si powders	-----	18
Chapter 4. SYNTHESIS OF SILICON NANOWIRES BY MICROWAVE HEATING		
4.1. Synthesis of Si nanowires from Si wafers	-----	22
4.2. Synthesis of Si nanowires from Si thin films	-----	24
REFERENCES	-----	26
APPENDIX A ~ E		

Chapter 1. INTRODUCTION

Portable electronic devices rely on portable power sources. Li batteries have been the centerpiece of cellular phones, notebook computers, camcorders, digital cameras, etc. Li is positioned right below hydrogen in the Periodic Table, so batteries built upon other materials cannot surpass the capacity of Li batteries.

Graphite is now widely used as the anode material in Li ion batteries. However, the theoretical capacity of graphite having LiC_6 composition is only 372 mAh/g, which can be reached within 0-300 mV versus metallic Li[1, 2]. Therefore, research to change the graphite to a high performance material is essential to develop the next-generation, high-performance Li ion battery.

The anode material for the next generation Li ion battery should be one that can be alloyed with Li. Sn, Al and Si have much higher theoretical capacities than graphite, with Si in the $\text{Li}_{4.4}\text{Si}$ formation having the highest theoretical capacity, 4200 mAh/g[3]. However, immense volume changes happen in the Li alloy anode. In case of Si, as Li insertion and extraction continues, the performance fades rapidly because of volume change of about 310% taking place during charging and discharging[4].

In this report, we have investigated the morphological change of the Si electrodes during repeated charging and discharging, and tested novel ideas to circumvent or avoid the capacity decrease with the cycle number.

Chapter 2. SILICON THIN FILM ANODES (Related data : Appendix A)

Si materials have been heavily studied to overcome the poor cycleability while improving the capacity. This research has focused on reducing the size of active materials or on highly dispersing the active materials to reduce the extent of local volume changes during cycling[5-15]. Other approaches have been to add a cushioning material to effectively offset the volume change of the active materials[16-30]. Figure 1 shows the specific capacities from 33 different studies as a function of cycle number. Interestingly, Si thin films not containing any inactive material have the highest known capacities, except for one study[31-37].

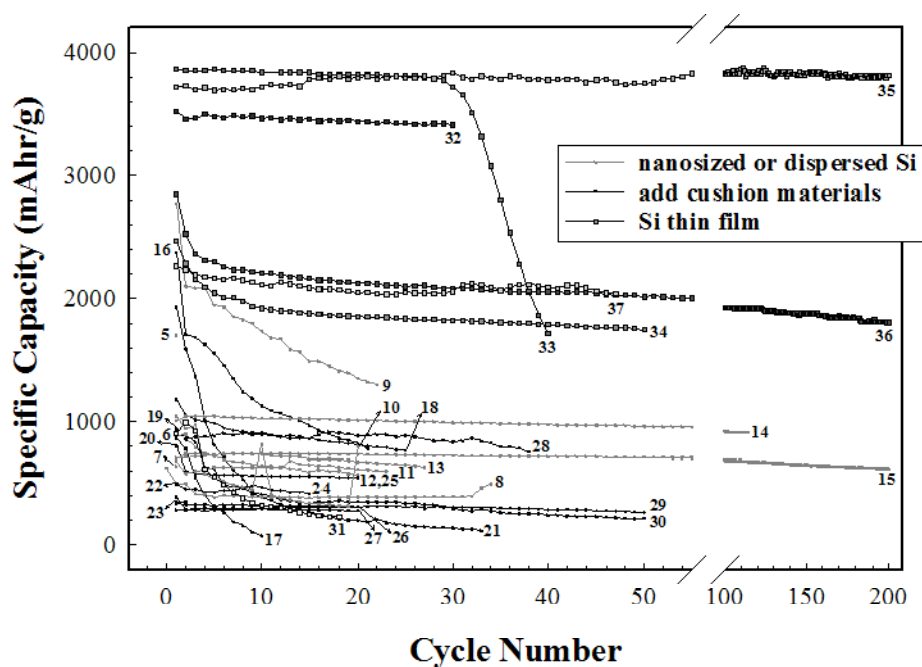


Figure 1. Specific capacities from 33 different studies as a function of cycle number[5-37].

Unfortunately, capacity decreases with cycle number are obvious in most of Si thin film electrodes. This is mainly because there is no mechanism to relieve the stress generated by volume expansion in a thin film system. On the other hand, it is generally known that the flexibility of a material increases with decreasing thickness. Therefore, the effect of Si film thickness should be investigated for the development of batteries with high capacities. Here, the thickness–cycle number relationship is reported for Si anodes, and the main reasons for the capacity decrease with increasing cycle number are investigated.

Si electrodes were prepared by rf magnetron sputtering a Si target (4 in. in diameter) at 5.0×10^{-3} torr with Ar gas onto 18 μm thick Cu foil as a current collector. The other sputtering conditions were an RF power of 150 W, and 100 rpm rotation. The film thickness was controlled by varying the sputtering time, and measured by an Alpha-step (Model 500, surface profiler, 230V, 50Hz, KLA Tencor).

The surface morphology of samples was observed by FE-SEM (S-4200, Hitachi, or XL 30S FEG, PHILIPS) and AFM (Dimension 3100, Digital Instruments Inc.). The Energy dispersive X-ray spectroscopy (EDS) analyzer which was attached to the SEM (XL 30S FEG, PHILIPS) unit was used to investigate the composition of the samples.

The electrochemical properties of the electrodes were evaluated by fabricating electrochemical cells in a glove box filled with dried argon gas at ambient temperature. The beaker type cell consisted of the Si working electrode, Li metal as the counter and the reference electrodes, and 1M LiPF_6 in EC:DMC (Ethylene carbonate plus diethyl carbonate as 1:1 in volume, Cheil Ind.) electrolyte. It was sealed tightly to protect it from the surrounding environment and then moved from the glove box to carry out electrochemical tests. The electrochemical properties were measured using a charge-discharge battery cycler (WBCS 3000, WonA Tech) in the voltage range of 1.5 V to 0.02 V. A 0.25C constant current rate was employed on the basis of the theoretical capacity of Si (1C = 4000 mAh/g) with a 60 sec rest period between every charge/discharge cycle.

Since the film thickness is an important variable in this study, precise control of the

film thickness must be achieved. Figure 2 shows the perfectly linear relationship between the film thickness and sputtering time in our sputtering system. We confirmed that the film thickness varied at a rate of $0.5 \text{ \AA}/\text{sec}$ after calibration during sputtering. The pristine Cu foil is sample A.

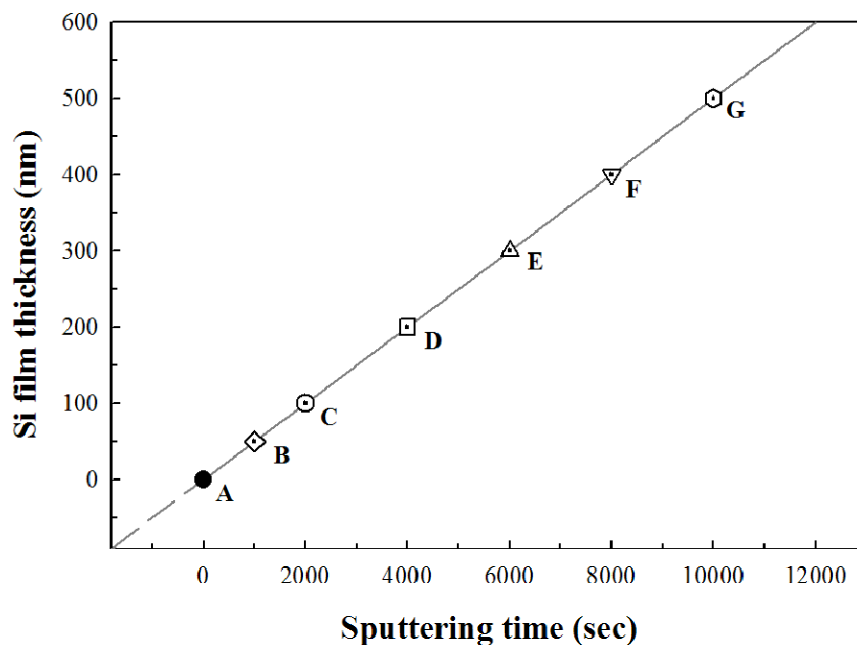


Figure 2. The thicknesses of the Si film electrodes as a function of sputtering time.

SEM and AFM images of the Si film electrodes are presented in Figure 3. These images show that the striped pattern present on the pristine Cu foil is maintained when the Si film is sputtered over it. The root mean square (RMS) roughness value of sample A was about 24 nm. It varied slightly with the positions of AFM measurements. There was little roughness change of the Si film electrodes with increasing sputtering time.

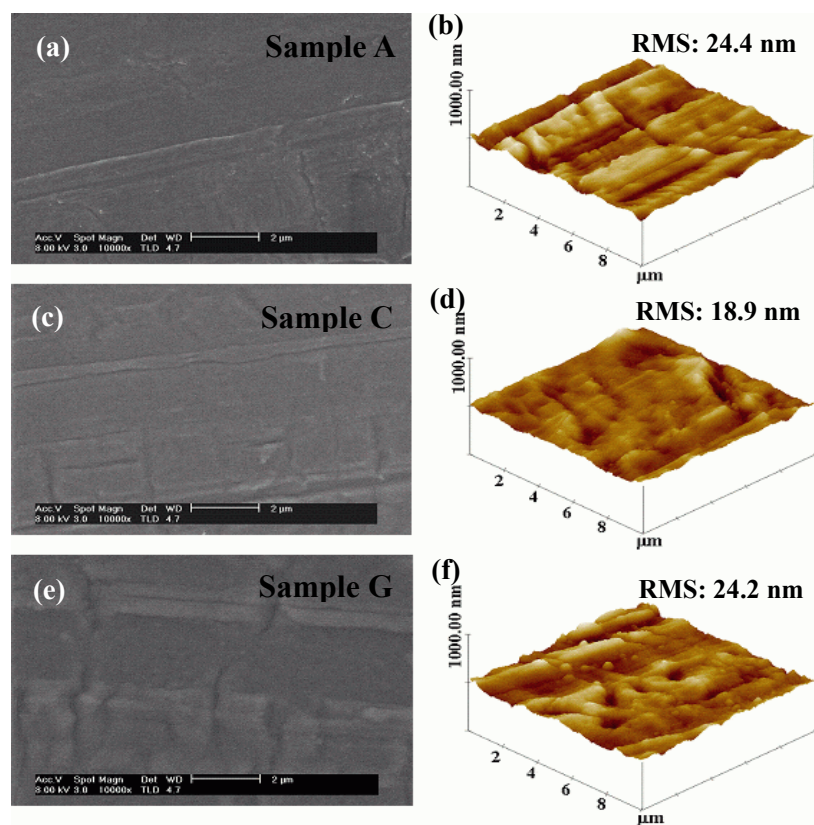


Figure 3. The surface morphology of the Si film electrodes: (a and b) sample A (pristine Cu foil); (c and d) sample C; (e and f) sample G.

Figure 4 plots the capacity of the first cycle during Li insertion and extraction with the film thickness. This very important factor shows how much irreversibility the cell possesses, namely the ratio of the Li extraction per Li insertion. As the film thickness increases, both the insertion and the extraction amounts decrease. This fact clearly indicates the advantage of using thinner Si films or smaller Si particles as anode materials. The capacity of the first cycle of sample F is 1722 mAh/g (charge) / 1283 mAh/g (discharge), which is half the value (2831 mAh/g / 2603 mAh/g) of sample C, and the capacity of sample G is surprisingly small. However, the irreversible capacity is not affected directly by the thickness of the Si film.

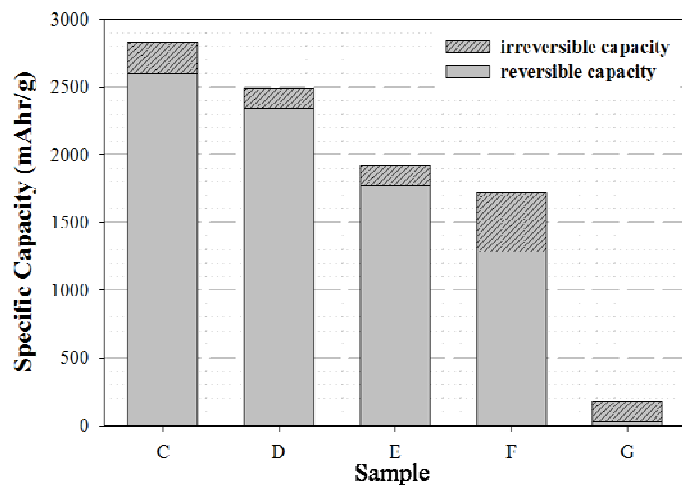


Figure 4. Reversible and irreversible (charge/discharge of first cycle) capacities of the Si film electrodes (sample C, D, E, F and G).

An EDS analysis was carried out to check for any side reaction on the surface of the electrode. However, Table 1 shows that only Cu, Si, O, and Ar were formed. Si increases, and Cu decreases as Si film thickness increases because the Cu foil surface was blocked by the Si film. O is probably the result of exposure to the atmosphere. A small amount of Ar was detected because we used an Ar plasma during the sputtering.

Table 1. Elemental analysis of the Si film electrodes.

Atomic %				
Elements	Sample A	Sample C	Sample D	Sample G
Si	-	42.09	62.96	90.46
Cu	92.54	50.24	29.71	3.37
O	7.46	7.67	5.66	4.51
Ar	-	-	1.67	1.65
Total	100	100	100	100

The cells were tested up to 50 cycles at a 0.25C rate, as shown in Figure 5. It indicates the discharge (Li extraction) capacity of each electrode with the cycle number. First, as Li insertion and extraction continues, the capacity decreases in every Si electrode regardless of the film thickness because repetitive Li insertion and extraction into the Si film induces deformation due to the immense volume change. Second, sample C performs the best among all electrodes. Third, samples B, C, D and E had capacity increases after the first cycles. This phenomenon can be explained as Li entering the Si film more easily by cracks arising from the volume change during the first cycle. Last, samples can be classified into three groups by graph shape. One group is samples B and C, which fade smoothly. Another is samples D, E, and F, which fade dramatically. The last one is sample G, which has almost no specific capacity. The reasons for these different behaviors will be discussed later in this paper.

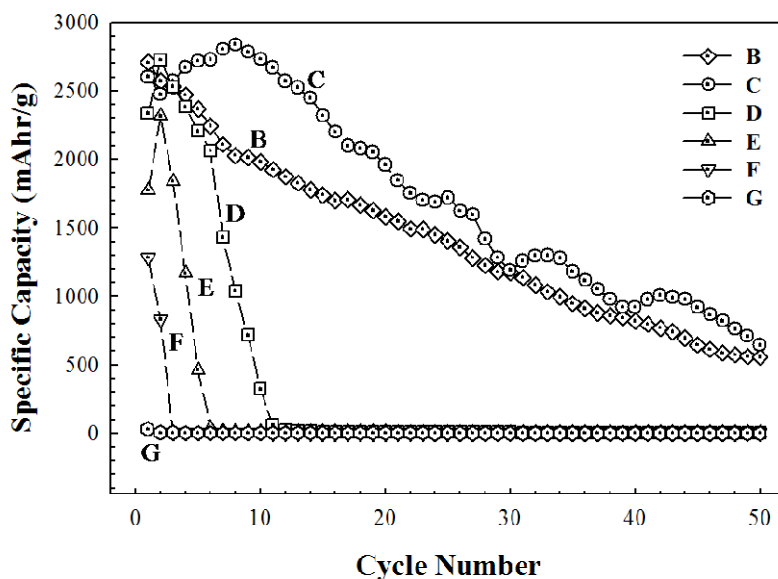


Figure 5. Discharge capacity vs. charge/discharge cycle number for the Si film electrodes at 0.25C rate.

Figure 6 shows the voltage profile through charge/discharge of samples C and D, which behaved quite differently in Figure 5. Figure 6(a) shows that Li extraction (discharge) decreases 228 mAhr/g less than Li insertion (charge). The 1st Li insertion (charge) has a plateau near 0.3 V and then Li insertion happens with a gentle slope. The capacity slowly increases to the 10th cycle (refer to Figure 5), but after that it decreases. In the 30th cycle, the capacity is less than half that of the first one. In sample D, which is twice as thick as sample C, the 1st Li insertion (charge) has a plateau near 0.2V and then the voltage declines. The 1st Li insertion (charge) shows a plateau like Figure 6(a), but we can not observe the plateau at the 2nd insertion. This indicates that the material behaves as though it were composed of a single phase over a wide range of composition [38, 39]. However, the definite difference between samples D and C is that sample D cannot function as early as the 10th cycle.

Figure 7 shows the morphology changes of sample C through charge and discharge. After the 5th cycle, we can see cracks in the film in Figure 7(b). Note that even though cracks are formed, the film is still attached to the Cu foil up to this stage. As the Si film is stressed continuously by volume change during charge/discharge, crumbling and pulverization occur, as in Figure 7(c) and (d). The bare Cu foil is exposed in several places due to the detachment of small Si pieces. Crack formation is also accelerated by the formation of intermetallic Li phases (Zintl phases) which are brittle [40].

On the other hand, different behaviors can be observed with sample D and sample F in Figure 8. Arrows 1 and 2 indicate the exposed Cu foil resulting from the detachment of Si pieces and delaminated Si films, respectively. We can observe crumbling and delamination in Figure 8(b) after the 5th cycle, while they are more prominent in Figure 8(d) after just the 1st cycle. This confirms that as sputtering time increases (as the film thickness increases) delamination becomes dominant.

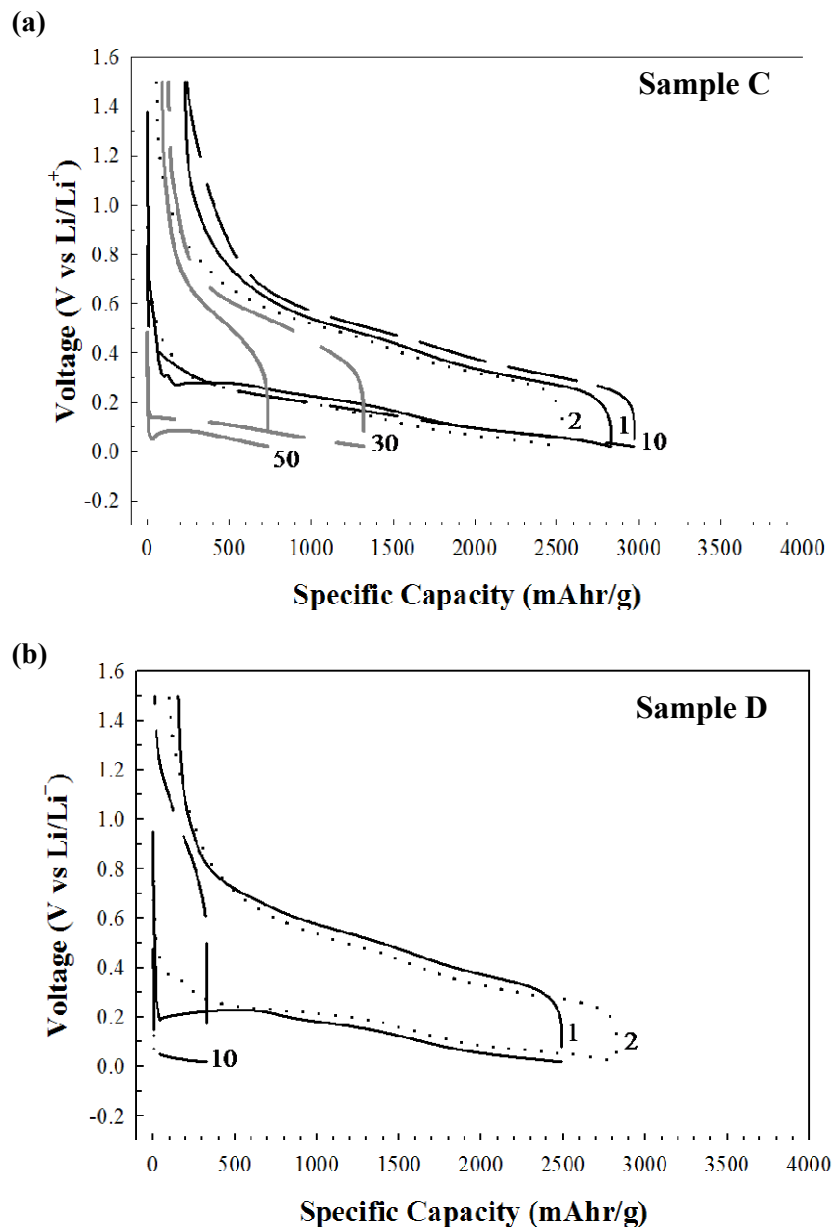


Figure 6. Voltage profiles of cycles 1, 2, 10, 30 and 50 for the Si film electrodes: (a) sample C; (b) sample D.

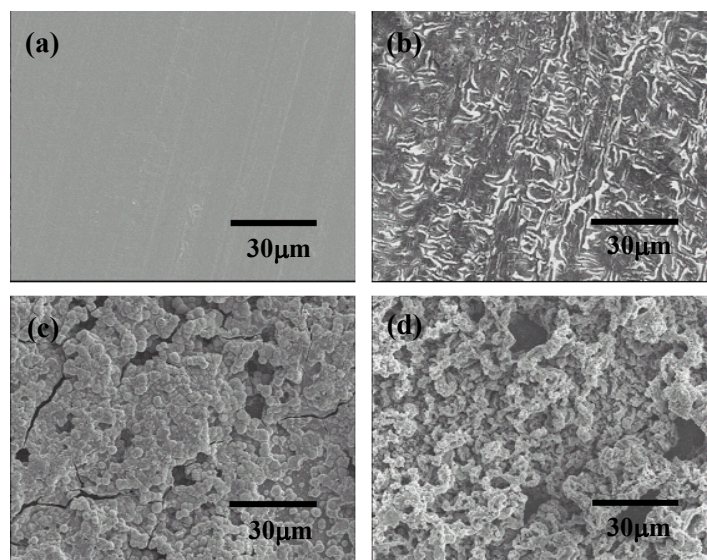


Figure 7. Change of the surface morphology of the Si film electrode (sample C) as cycle test proceeds: (a) before cycles, (b) after 5th, (c) after 10th, and (d) after 30th charge/discharge cycle at a 0.25C rate.

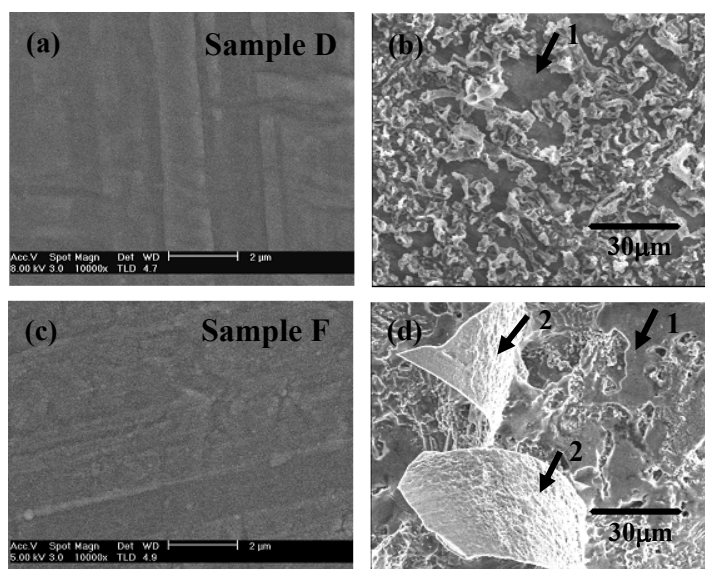


Figure 8. Change of the surface morphology of the Si film electrodes as cycle test proceeds: (a) before cycles (sample D) (b) after 5th charge/discharge cycle of sample D, (c) before cycles (sample F), (d) after 1st charge/discharge cycle of sample F at a 0.25C rate.

Figure 9 depicts the different deformation behaviors of Si electrodes deduced from this research. At first, volume expansion during Li insertion and extraction generates mechanical stress. When the strain energy (generated due to the volume difference between phases) equals or exceeds that required for the creation of new fracture surfaces, the new fractured surface is formed by receiving the energy from the Si film expansion (namely, volumetric stress) [41].

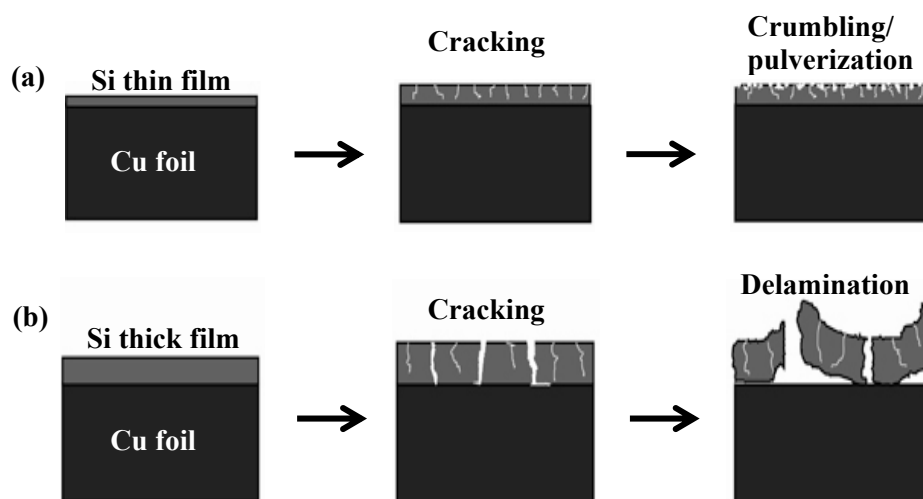


Figure 9. Schematic of the change of surface morphology of Si film electrodes.

(a) crumbling/pulverization at or below 100nm, and (b) delamination at or above 200nm with cracking induced by volume expansion.

As Li insertion/extraction proceeds cyclically, stress due to volume change causes crumbling/pulverization and/or delamination. The crumbling/pulverization occurred when the sputtered Si film electrode was about 100 nm thick or less. The active material, Si, becomes small pieces that gradually fall away. Thus, the capacity of the electrodes showing crumbling and pulverization decreases gradually.

Delamination is the dominant phenomenon in the films of at least 200 nm thickness. Adhesion failure occurs when the interfacial strain is less than the crack strain of a brittle film [42]. The adhesion energy is constant regardless of the film thickness, but the critical

force for adhesion failure is a function of film thickness. At the same adhesion energy, a thicker film has a smaller critical force than a thinner one. Furthermore, the total stress induced by volume expansion increases with film thickness. For these reasons, delamination happens dominantly in thicker Si films, and it causes the capacity to decrease sharply.

In summary, Si has the largest theoretical capacity of any anode material of Li batteries. Its large volume change, however, results in degradation of the capacity with repeated charging and discharging. The degradation mechanism is studied systematically in this paper.

When Li inserts into the Si film, it forms the brittle Zintl phase that is accompanied by a large volume change. The stress thus generated promotes crack formation which is responsible for the initial increase of the capacity of Si film electrodes.

The critical force for adhesion failure, which is a function of film thickness, is responsible for the following decrease of capacity. A thinner film has a larger critical force than a thicker one. The active material, Si, forms small pieces that gradually fall away in a thin Si film, resulting in a slow decrease of the capacity. On the other hand, the critical force is smaller in a thicker Si film. The increase in total stress is also responsible for the delamination and, thus, the rapid decrease of the capacity in a thicker Si film.

Appendix A reports all the raw data for the Si thin film electrodes. The surface treatment of current collectors can enhance the adhesion of Si films on the current collectors, and control the grain size of the Si thin films. Cu foils (supplied by LG Chem.) of 18 μm thickness were used as the current collectors. They were etched in 98.08% H_2SO_4 (Matsunoen chemicals) for 24 hours, and washed with distilled water, then completely dried before Si deposition. Cu foils with rough surfaces can increase surface area, thus surface energy and electric conductivity. Sputtering of Si on a rough surface results in a large number of connected Si lumps instead of a flat, continuous Si film. This structure is known to be beneficial to relieve the stress of volume expansion during Li insertion.

Chapter 3. SILICON NANOWIRES AS AN ANODE MATERIAL OF LITHIUM BATTERIES

3.1. Introduction

Many studies have been made with Si materials to overcome the poor cycleability while improving the capacity. Majority of previous studies have been focused on reducing the size of active materials to reduce the extent of local volume change during cycling. Smaller Si particles are known to be advantageous, though the contact resistance increases with the increased surface area of smaller particles. In this report, we have tested the potential of a new kind small Si particle, silicon nanowire, as an anode material of Li batteries.

3.2. Synthesis of Si nanowires from Si wafers

(Related data : Appendix B)

Si nanowires are typically synthesized using chemical vapor deposition method. The precursor materials, silane compounds, however, are dangerous materials; flammable and hazardous to human health. Therefore, Si nanowires were synthesized from Si wafers in our work. This method is safe, virtually immune to contamination, and very simple.

5 nm of Ni layer was deposited on the (111) oriented silicon wafer (p-type) by sputtering, and Si nanowires were synthesized by thermal heating under flowing Ar and H₂(10%) atmosphere.

Figure 10 show the SEM image of the sample heated at 990 °C for 2 hours. We can observe Si nanowires of 10~50 nm diameters, but majority of them lies between 20 to 30 nm. The Cs-corrected TEM (JEM-2100F) image of one Si nanowire appears in Figure 11. As denited in Fig. 11(a), this Si nanowire has a 23nm diameter. Fig. 11(b) is the magnified image of the part of the same nanowire, which is marked as a square in Fig. 11(a). We can confirm that this Si nanowire has amorphous structure.

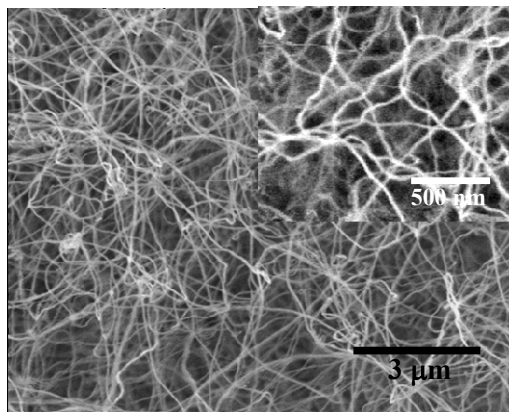


Figure 10. SEM images of Si nanowires synthesized at 990 °C for 2hr.

Inset: high magnification.

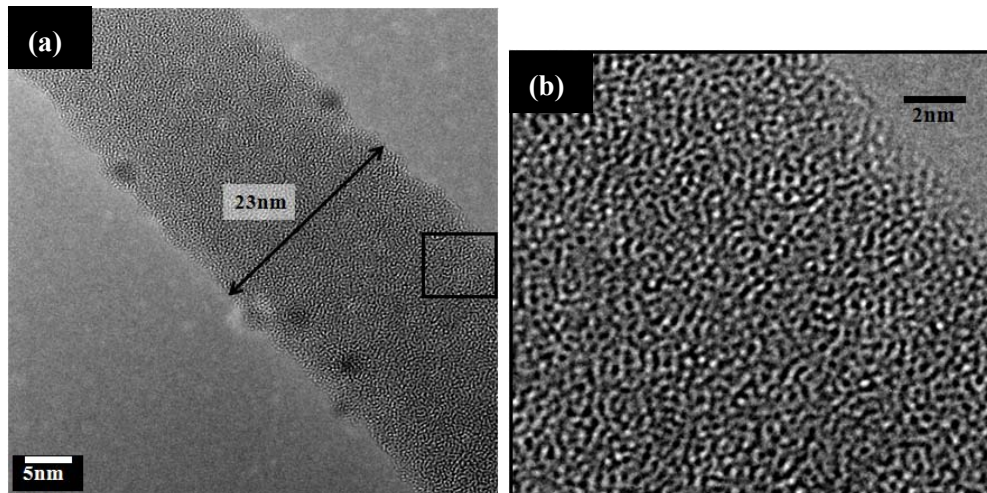


Figure 11. HR-TEM images of Si nanowire synthesized at 990 °C for 2hr.
 (a) Low magnification and (b) High magnification

Cu foils of 18 μm thickness were etched in 98.08% sulfuric acid (Matsunoen Chemicals) for 24 hours, and rinsed with DI water, then completely dried. Si nanowires were dispersed in ethanol using sonication, and then electrodes were fabricated by spraying the solution on the Cu foil. The electrodes were finally dried in a vacuum oven at 120°C for 12 hours.

Figure 12 shows the morphology and the composition of the Si nanowires electrode on the Cu substrate. Si nanowires are uniformly deposited throughout the electrode with a high density. The elemental analysis also proves that the Si nanowires electrode is successfully fabricated. The carbon in this Table comes from the carbon tape used for the preparation of the sample for EDS measurement, while Cu comes from the Cu current collector. Note that the high percentage of oxygen. Si nanowires take up 25 atomic % of oxygen from air due to the large surface area. Oxygen atoms mainly present either as a silicon oxide or as various surface functional groups, so they have a considerable effect on the performance of the Si nanowire electrode.

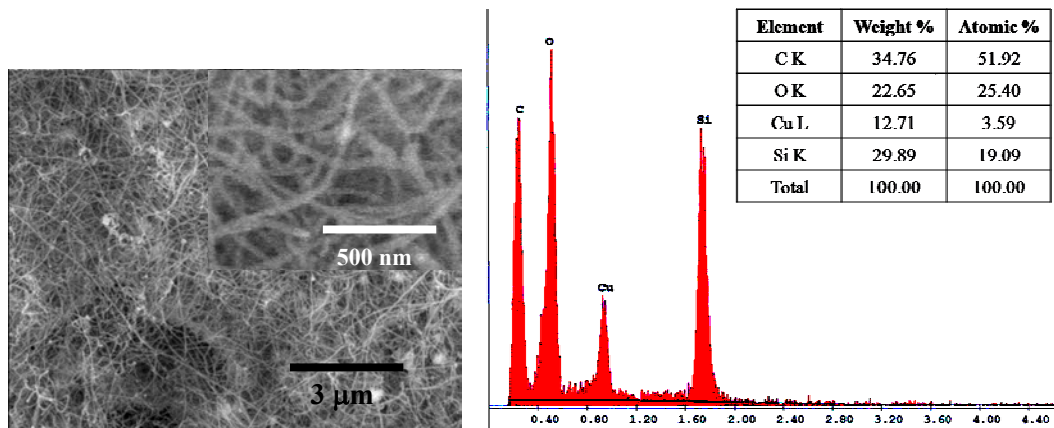


Figure 12. SEM images and EDS analysis of the fabricated Si nanowires electrode.

The specific capacity of a Si nanowire electrode is shown in Figure 13 as a function of cycle number. The Si nanowire electrode has a large specific capacity of 2900 mAh/g during Li insertion, but it reduces to 500 mAh/g during Li extraction in the first cycle. The irreversible capacity of 2400 mAh/g is a surprisingly large value. Likely reasons are presence of oxygen on the surface of Si nanowires and the decrease in electrical conductivity due to Li insertion. Li forms a stable Li_2O phase when it is exposed to oxygen, which is responsible for the high irreversible capacities [16, 43, 44]. However, Li_2O has its own merits such as alleviation of volume expansion [45] and as a Si particle binder during cycling [14]. These merits are also observed in our result. The specific capacity reduces very slowly with the cycle number in Figure 13 from the initial discharge (Li extraction) value. The charge/discharge capacity of the 30th cycle is almost 72% of the discharge capacity of the 1st cycle.

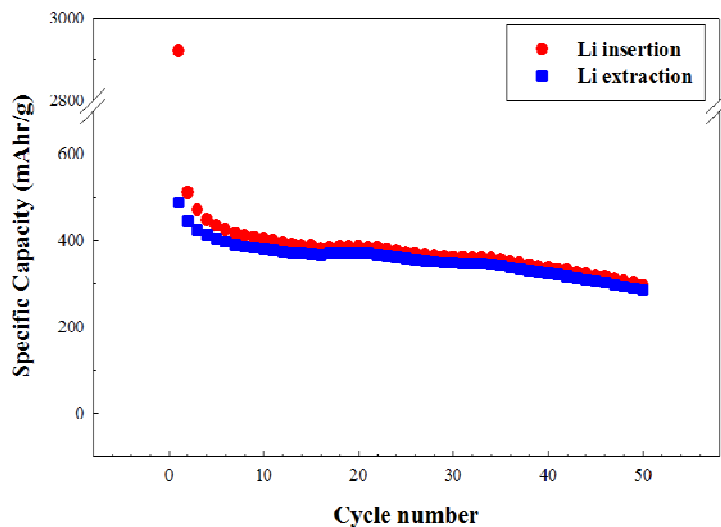


Figure 13. Specific capacity vs. cycle number for the Si nanowires electrode at 0.25C rate.

Large irreversible capacity is a major demerit, and must be cured. A widely investigated cure for Si powders, carbon coating, can also be applied to Si nanowires. Merits of carbon coating include 1) stabilization of the surface of Si nanowires by blocking oxygen, 2) increased electrical conductivity, and 3) as a cushion material to relieve the stress of volume expansion. We are now investigating the effect of carbon coating on Si nanowires, and preliminary results are included as Appendix D, though such investigation is out of the scope of this report.

3.3. Synthesis of Si nanowires from Si powders

(Related data : Appendix C)

In the previous section, Si nanowires were synthesized from Si wafers. Although Si wafers are a perfect raw material to synthesize Si nanowires, they are very expensive and the amount of synthesized Si nanowires is rather small to fabricate large area electrodes. A byproduct of Si wafers, Si powders, have almost the same purity of Si wafers, and very cheap. Comparing with equal weight, they have much larger surface area due to the small particle size than Si wafers, so that the productivity of Si nanowires from Si powders far surpass that from Si wafers.

2.112g of silicon powders (average diameter 2.64 μ m) were mixed with 80ml of a 0.1M aqueous solution of Ni(NO₃) \cdot 6H₂O and vigorously stirred for 30 min. The water was evaporated in a rotary evaporator and the solid remnants were completely dried in an oven at 150°C. The final sample (Ni-impregnated Si powders) was obtained by grinding the solids in a mortar.

0.03g of Ni-impregnated Si powders were put in a quartz boat, and the boat was placed in a thermal furnace. The sample was reduced at 500°C for 4 hours under flowing Ar (180 sccm) and H₂(20sccm), then the temperature was raised to 990°C to synthesize Si nanowires.

0.1g of the reacted Si powders were mixed with 10ml ethanol and, then, they were dispersed in ethanol using sonication for 1 hour. Si nanowires were separated from the Si powders by centrifuge at 5000 rpm for 10 min.

The separated Si nanowires were redistributed in ethanol with the addition of 0.1g/l of NiCl₂ to add positive surface charge to the Si nanowires. The electrophoretic depositions of Si nanowires on Ni current collectors were carried out by applying 1~9 V (2~18 V/cm) of DC current for an hour between the Pt positive electrode and the Ni negative electrode.

To evaluate electrochemical properties of the Si nanowire electrodes,

electrochemical cells were fabricated in a glove box filled with dried argon gas at ambient temperature. The beaker type cell consisted of the Si working electrode, Li metal as the counter and the reference electrodes, and 1M LiPF₆ in EC:DMC (Ethylene carbonate plus diethyl carbonate as 1:1 in volume, Cheil Ind.) electrolyte. It was sealed tightly to protect it from the surrounding environment and then moved from the glove box to carry out electrochemical tests. The electrochemical properties were measured using a charge-discharge battery cycler (WBCS 3000, WonA Tech) in the voltage range of 1.5 V to 0.02 V. A 0.25C constant current rate was employed on the basis of the theoretical capacity of Si (1C = 4000 mAhr/g) with a 60 sec rest period between every charge/discharge cycle.

Figure 14 shows the morphology and microstructure of a Si nanowire. Amorphous nature of the Si nanowire is surely confirmed in this Figure.

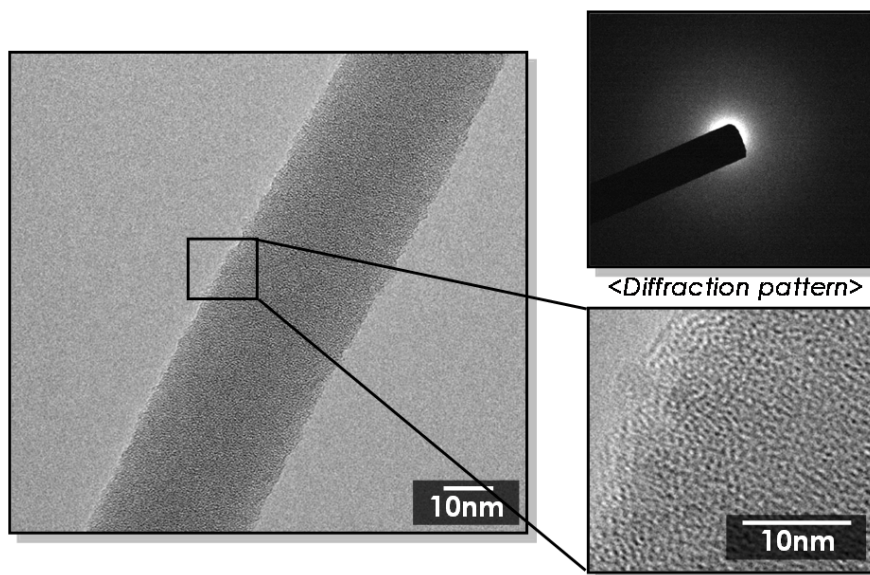


Figure 14. Morphology and microstructure of a Si nanowire synthesized from the Si powders.

Figure 15 is the SEM image of a Si nanowire electrode fabricated by using electrophoretic deposition. This particular electrode was deposited at 5V(10V/cm) for 1 hour, and uniform deposition is confirmed. Figure 15 (b) is the result of repeated charge/discharge experiments using the Si nanowire electrode shown in Figure 15 (a). The electrochemical performance of this electrode is extremely poor. We have no idea why it shows such a disappointing performance. We are now doing in-depth investigation about each fabrication step as well as the Si nanowires themselves. All of the raw data are given in the Appendix C.

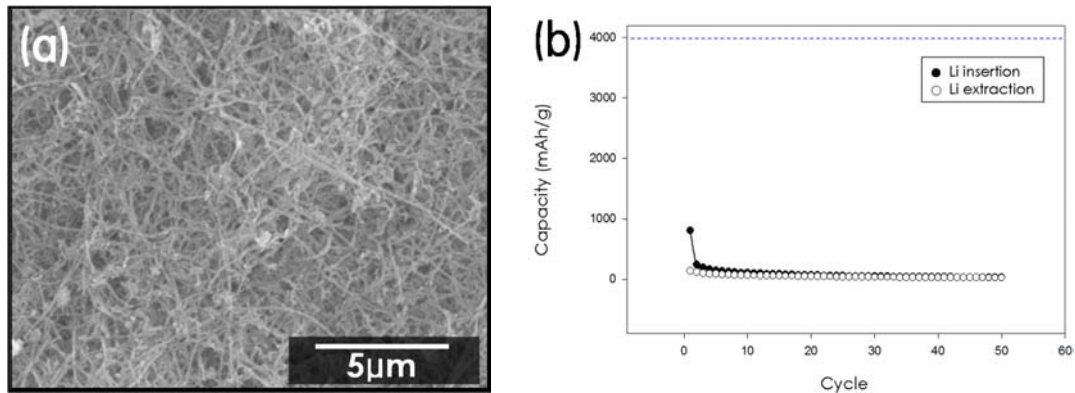


Figure 15. Si nanowire electrode deposited by electrophoretic deposition at 10V/cm for 1hr. (a) surface morphology (b) electrochemical performance

Chapter 4. SYNTHESIS OF SILICON NANOWIRES BY MICROWAVE HEATING

Nanowires are promising candidates for the quantum electronics of the 21st century. They are easy to be synthesized, diverse in composition and properties, and well-defined in the crystalline structures. Some nanowires, especially amorphous silicon nanowires, are expected to be the material of the next generation lithium batteries which boast a 10-fold capacity increase from today's state-of-the-art lithium-ion batteries.

The standard technique to synthesize nanowires is chemical vapor deposition (CVD). CVD can produce high quality nanowires of various materials, though some limitations – precursor synthesis, vacuum equipment, small size - are present. Incorporation of small amount of impurity is inevitable in some cases due to the lack of appropriate precursors. Some techniques are free from these limitations. Gold catalysts on the surface of a silicon wafer can transform the underlying silicon wafer into silicon nanowires through solid-liquid-solid (SLS) transition by simple heating at inert atmosphere.

Microwaves can also be used in the synthesis of various nanowires. The merits of microwave synthesis of CNTs – fast, clean, applicable to a large area, and atmospheric operation – still remains in the case of nanowires. Note that microwave synthesis is expected to grow nanowires on various substrates including glasses and organic polymers, which is unlikely to be achieved by using conventional heating technique. In this research, we report the potential of microwave synthesis as a method of producing highly pure silicon nanowires.

A large portion of the Chapter 4 is identical to the report submitted in the previous year. However, we have included some additional data (Figs 9~11 in Appendix D) in this section. Especially, carbon coating of Si nanowires is an interesting idea and has a potential to solve some serious problems associated with nanosized Si wires, so that we have included some raw data. A full-scale investigation is in progress now.

4.1. Synthesis of Si nanowires from Si wafer

(Related Data : Appendix D)

In this experiment, Si wafer was used as the solid silicon source, and gold was used as a catalyst. A P-type Si (100) wafer was sputtered with gold to form a thin gold film of 40 nm thickness. (RF power : 100W, rotation : 100rpm, working pressure : 5.0×10^{-3} torr) The sample was placed in the reaction chamber of the microwave irradiation system, and the reaction chamber was purged with flowing Ar. Then, Ar was changed to a gas mixture of 180 sccm Ar and 20 sccm H_2 during microwave irradiation. The pressure of the reaction chamber was maintained at 1 atm during reaction.

Figure 16(a) shows the morphology of the sample after microwave irradiation of 40 sec with the forward power of 400W and no reflected power. Fibrous structures with the diameters in the range of 10~50 nm can be observed in this Figure. The microstructure of a nanowire was revealed by using HR-TEM in Figure 16(b). This particular nanowire is made of amorphous silicon, and the diameter is about 40nm.

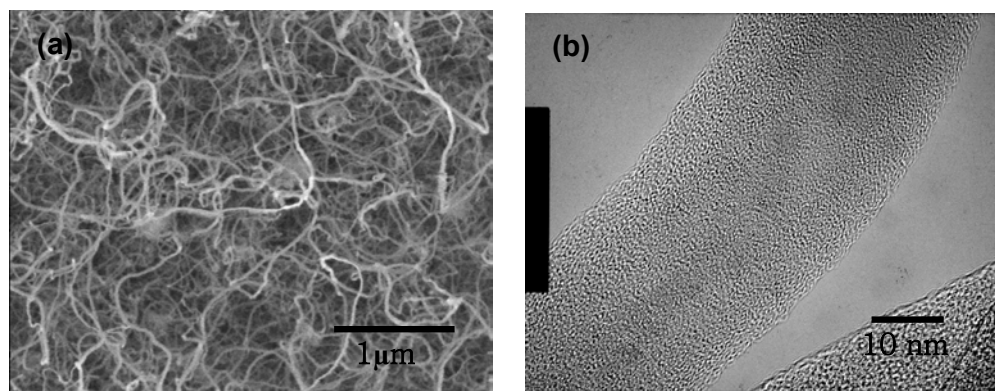


Figure 16. Images of Si nanowires from a Si wafer by microwave irradiation at 400 W for 40sec.

(a) Morpholgy observed by FE-SEM

(b) Microstructure observed by HR-TEM

The mechanism of the formation of silicon nanowires is schematically given in Figure 17 with corresponding SEM photographs. Thin gold film transforms into gold nanoparticles, and these gold nanoparticles play a role of catalyst for the growth of Si nanowires.

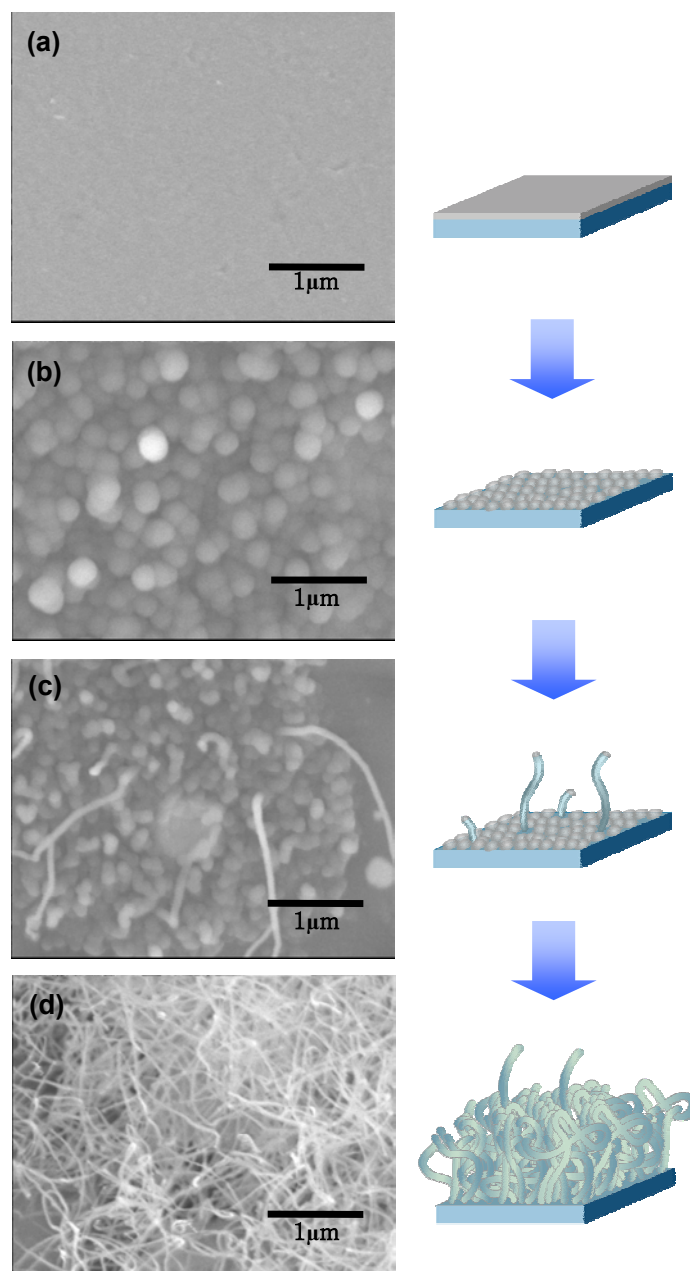


Figure 17. Mechanism of Si nanowires formation

4.2. Synthesis of Si nanowires from Si thin films

(Related Data : Appendix E)

Identical experiment was repeated with the thin silicon film on a quartz wafer. 2 μm of thin Si film was deposited using the sputter on a quartz wafer, followed by the deposition of 40 nm of thin gold layer. The sample was placed in the reaction chamber of the microwave irradiation system, and the reaction chamber was purged with flowing Ar. The pressure of the reaction chamber was maintained at 1 atm during reaction.

Figure 18(a) shows the morphology of the sample after microwave irradiation of 60 sec with the forward power of 800W and the reflected power of 400W. Fibrous structures with a wide diameter variation can be observed in this Figure. The microstructure of a nanowire was revealed by using HR-TEM in Figure 18(b). This particular nanowire is made of amorphous silicon, and the diameter is about 25nm.

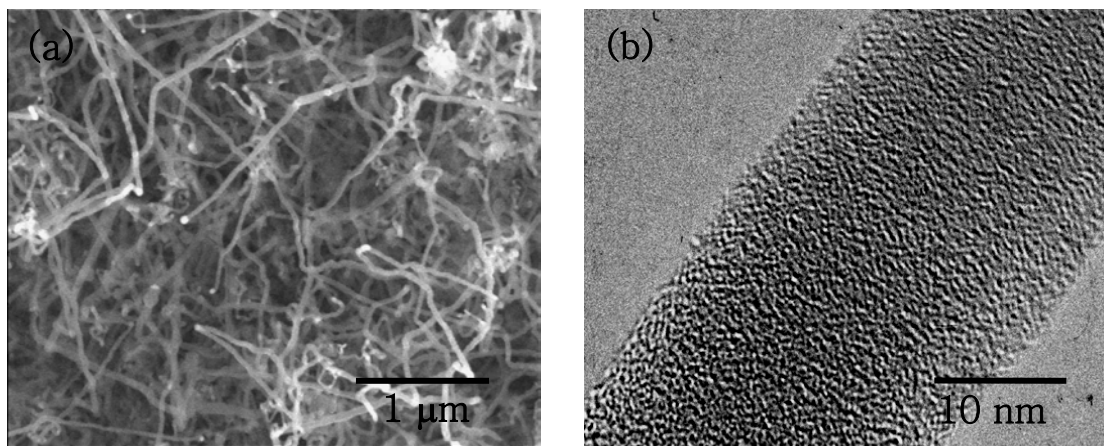


Figure 18. Images of Si nanowires from a Si film by microwave irradiation at forward power 800 W and reflected power 400 W for 60sec.

(a) SEM image

(b) HR-TEM image

Similar experiments were repeated with the thin silicon film on Teflon sheets. 10 nm of titanium layer was first deposited using the sputter on the surface of a Teflon sheet to guarantee good adhesion. Then, 2 μm of thin Si film was deposited, followed by the deposition of 40 nm of thin gold layer. The sample was placed in the reaction chamber of the microwave irradiation system, and the reaction chamber was purged with flowing Ar. The pressure of the reaction chamber was maintained at 1 atm during reaction.

Figure 19 shows the morphology of the sample after reaction. Short fibrous nanostructures are formed with round particles on their ends. Electron diffraction study reveals that these nanostructures are primarily made of silicon. Although further study must be followed, it proves the possibility of the synthesis of Si nanowires on a flexible substrate. This technology will be able to provide flexible batteries with a high energy density in the years to come.

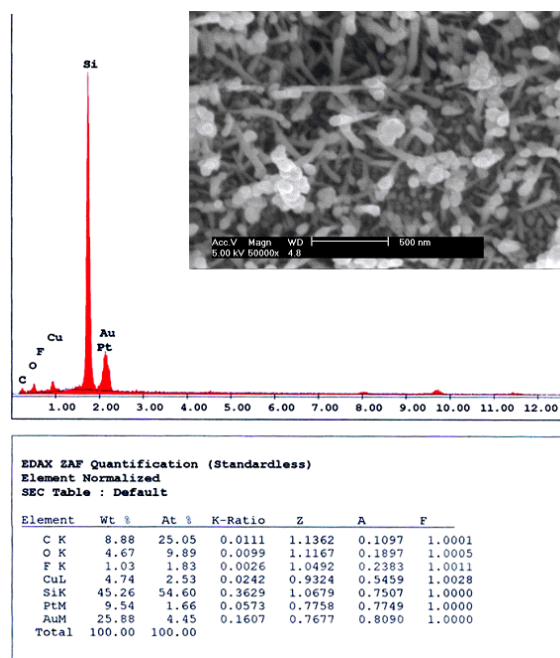


Figure 19. EDS spectra of synthesized Si nanowires. The inset is the SEM image of the nanowires.

REFERENCES

1. B. Simon, S. Flandrois, K. Guerin, A. Fevrier-Bouvier, I. Teulat, P. Biensan, J. Power Sources 81/82 (1999) 312
2. Tsutomu Ohzuku, Yasunobu Iwakoshi, and Keijiro Sawai, J. Electrochem. Soc. 140 (1993) 2490.
3. Noriyuki Tamura, Ryuji Ohshita, Masahisa Fujimoto, Maruo Kamino and Shin Fujitani, J. Electrochem. Soc. 150 (2003) A679.
4. L.Y. Beaulieu, K.W. Eberman, R.L. Turner, L.J. Krause, and J.R. Dahn, Electrochem. Solid-State Lett. 4(9) (2001) A137.
5. G.W. Zhou, H. Li, H.P. Sun, D.P. Yu, Y.Q. Wang, X.J. Huang, L.Q. Chen, Z. Zhang, Appl. Phys. Lett. 75 (16) (1999) 2447
6. A.M. Wilson, B.M. Way, J.R. Dahn, J. Appl. Phys. 77 (6) (1995) 2363
7. Weibing Xing, A.M. Wilson, G. Zank, J.R. Dahn, Solid State Ionics 93 (1997) 239
8. A.M. Wilson and J.R. Dahn, J. Electrochem. Soc. 142 (2) (1995) 326
9. Hong Li, Xuejie Huang, Liquan Chen, Zhengang Wu, and Young Liang, Electrochem. Solid-State Lett. 2 (11) (1999) 547
10. C.S. Wang, G.T. Wu, X.B. Zhang, Z.F. Qi, W.Z. Li, J. Electrochem. Soc. 145 (8) (1998) 2751
11. Z.S. Wen, J. Yang, B.F. Wang, K. Wang, Y. Liu, Electrochem. Commun. 5 (2003) 165
12. Tatsuo Umeno, Kenji Fukuda, Hongyu Wang, Nikolay Dimov, Takashi Iwao, Masaki Yoshio, Chem. Lett. (2001) 1186
13. J. Yang, B.F. Wang, K. Wang, Y. Liu, J. Y. Xie and Z.S. Wen. Electrochem. Solid-State Lett. 6 (8) (2003) A154
14. Michael Holzapfel, Hilmi Buqa, Werner Scheifele, Petr Novák, Frank-Martin Petrat, Chem. Commun. (2005) 1566
15. Tomokazu Morita, Norio Takami, J. Electrochem. Soc. 153 (2) (2006) A425

16. J. Yang, Y. Takeda, N. Imanishi, C. Capiglia, J.Y. Xie, O. Yamamoto, *Solid State Ionics* 152-153 (2002) 125
17. Hansu Kim, Junghee Choi, Hun-Joon Sohn and Tak Kang, *J. Electrochem. Soc.* 146 (12) (1999) 4401
18. G.X. Wang, L. Sun, D.H. Bradhurst, S. Zhong, S.X. Dou, H.K. Liu, *J. Power Sources* 88 (2000) 278
19. H. Huang, E.M. Kelder, L. Chen, J. Schoonman, *J. Power Sources* 81/82 (1999) 362
20. W.J. Weydanz, M. Wohlfahrt-Mehrens, R.A. Huggins, *J. Power Sources* 81-82 (1999) 237
21. S.B. Ng, Jim Y. Lee, Z.L. Liu, *J. Power Sources* 94 (2001) 63
22. D. Larcher, C. Mudalige, A.E. George, V. Porter, M. Gharghouri, J.R. Dahn, *Solid State Ionics* 122 (1999) 71
23. Gerko Oskam, Peter C. Searson, T. Richard Jow, *Electrochem. Solid-State Lett.* 2 (12) (1999) 610
24. H. Dong, X.P. Ai, H.X. Yang, *Electrochem. Commun.* 5 (2003) 952
25. Heon-Young Lee, Sung-Man Lee, *J. Power Sources* 112 (2002) 649
26. Il-seok Kim, G.E. Blomgren, P.N. Kumta, *Electrochem. Solid-State Lett.* 6 (8) (2003) A157
27. Il-seok Kim, P.N. Kumta, G.E. Blomgren, *Electrochem. Solid-State Lett.* 3 (11) (2000) 493
28. Zonghai Chen, L. Christensen, J.R. Dahn, *Electrochem. Commun.* 5 (2003) 919
29. Sung-Min Hwang, Heon-Young Lee, Serk-Won Jang, Sung-Man Lee, Seung-Joo Lee, Hong-Koo Baik, Jai-Young Lee, *Electrochem. Solid-State Lett.* 4 (7) (2001) A97
30. J. Wolfenstine, *J. Power Sources* 124 (2003) 241
31. S. Bourderau, T. Brousse, D.M. Schleich, *J. Power Sources* 81/82 (1999) 233
32. J.P. Maranchi, A.F. Hepp, P.N. Kumta, *Electrochem. Solid-State Lett.* 6 (9) (2003) A198
33. J.P. Maranchi, A.F. Hepp, A.G. Evans, N.T. Nuhfer, P.N. Kumta, *J. Electrochem. Soc.*

- 153 (6) (2006) A1246
34. J. Graetz, C.C. Ahn, R. Yazami, B. Fultz, *Electrochem. Solid-State Lett.* 6 (9) (2003) A194
35. Shigeki Ohara, Junji Suzuki, Kyoichi Sekine, Tsutomu Takamura, *J. Power Sources* 136 (2004) 303
36. Tsutomu Takamura, Shigeki Ohara, Makiko Uehara, Junji Suzuki, Kyoichi Sekine, *J. Power Sources* 129 (2004) 96
37. Makiko Uehara, Junji Suzuki, Kohki Tamura, Kyoichi Sekine, Tsutomu Takamura, *J. Power Sources* 146 (2005) 441
38. Hunjoon Jung, Min Park, Yeo-Geon Yoon, Gi-Bum Kim, Seung-Ki Joo, *J. Power Sources* 115 (2003) 346
39. Robert A. Huggins, *J. Power Sources* 81-82 (1999) 13
40. J. Yang, M. Winter, J.O. Besenhard, *Solid State Ionics* 90 (1996) 281
41. J. Wolfenstine, *J. Power Sources* 79 (1999) 111
42. T.S. Chow, C.A. Liu and R.C. Penwell, *J. Polym. Sci.: Polym. Phys. Ed.*, 14 (1976) 1305
43. Yasutaka Nagao, Hiroki Sakaguchi, Hitohiko Honda, Toshiharu Fukunaga, and Takao Esaka, *J. Electrochem. Soc.* 151(10) (2004) A1572
44. Weibing Xing, A. M. Wilson, K. Eguchi, G. Zank, and J. R. Dahna, *J. Electrochem. Soc.* 144(7) (1997) 2410
45. Yoshio Idota, Tadahiko Kubota, Akihiro Matsufuji, Yukio Maekawa, Tsutomu Miyasaka, *Sci. J.* 276 (1997) 1395